# Assembling the Building Blocks of Giant Planets around Intermediate Mass Stars

K. A. Kretke[1], D. N. C. Lin[1,2], P. Garaud[3], N. J. Turner[4]

[1]*Department of Astronomy and Astrophysics, University of California, Santa Cruz, CA, 95064*

[2]*Kavli Institute of Astronomy and Astrophysics, Peking University, Beijing, China*

[3]*Department of Applied Mathematics and Statistics, Baskin School of Engineering, University of California, Santa Cruz, CA, 95064*

[4] *Jet Propulsion Laboratory, California Institute of Technology, Pasadena, CA, 91109*

kretke@ucolick.org

## ABSTRACT

We examine a physical process that leads to the efficient formation of gas giant planets around intermediate mass stars. In the gaseous protoplanetary disks surrounding rapidly-accreting intermediate-mass stars we show that the midplane temperature (heated primarily by turbulent dissipation) can reach $\gtrsim$1000 K out to 1 AU. Thermal ionization of this hot gas couples the disk to the magnetic field, allowing the magneto-rotational instability (MRI) to generate turbulence and transport angular momentum. Further from the central star the ionization fraction decreases, decoupling the disk from the magnetic field and reducing the efficiency of angular momentum transport. As the disk evolves towards a quasi-steady state, a local maximum in the surface density and in the midplane pressure both develop at the inner edge of the MRI-dead zone, trapping inwardly migrating solid bodies. Small particles accumulate and coagulate into planetesimals which grow rapidly until they reach isolation mass. In contrast to the situation around solar type stars, we show that the isolation mass for cores at this critical radius around the more massive stars is large enough to promote the accretion of significant amounts of gas prior to disk depletion. Through this process, we anticipate a prolific production of gas giants at $\sim$ 1 AU around intermediate-mass stars.

*Subject headings:* planetary systems: formation, protoplanetary disks

## 1. Introduction

The discovery of a plethora of extra-solar planets around solar-type main sequence stars has established that planet formation must be a common process, not a peculiarity of our own solar system. As observational techniques for planetary detection have become more sophisticated, the discovery domain has expanded to include host stars with a wide range of masses. While on the main sequence, intermediate mass stars (stars with $1.5M_{\odot} \lesssim M_{*} \lesssim 3M_{\odot}$) make poor radial velocity (RV) survey candidates as they have few spectral lines which also tend to be rotationally broadened (Griffin et al. (2000) but see Galland et al. (2006)). However, once these stars evolve off the main sequence, their relatively cool and slowly rotating outer layers make them more suitable candidates for high precision spectroscopic studies. Recent RV surveys targeting evolved intermediate mass stars suggest that they differ from solar-type stars as planetary hosts in at least two respects. First, the total frequency of giant planets (with periods less than a few years) appears be higher around intermediate mass stars. Second, the planets have different statistical properties. Their semi-major axis distribution is concentrated at 1-2 AU and there is an apparent lack of short-period (days to months) planets, despite observational selection effects favoring their discovery (Lovis & Mayor 2007).

In this paper, we propose a common explanation for prolific gas giant formation with semi-major axes comparable to 1 AU and for the rarity of close-in planets around intermediate-mass stars. As it is unlikely that all planets within 1 AU have been engulfed or had their orbits disrupted by the current expanded envelope of the host stars (Johnson et al. 2007), we attribute both properties to the formation and early evolutionary processes rather than to post-main-sequence evolution.

We begin by examining the physical properties of circumstellar disks which may affect the probability of forming giant planets. In the core-accretion model of planet formation (cf. Bodenheimer & Pollack (1986)), the emergence of Jupiter-like gas giants requires that a population of solid cores form within a gaseous protoplanetary disk. These cores grow through cohesive collisions with planetesimals, with a growth rate determined by the velocity dispersion of the planetesimal swarm. The magnitude of this velocity dispersion is set by a balance between excitation by gravitational perturbations and damping by gas drag. In the gas-rich environment of typical protostellar disk, gas drag dominates so that field planetesimals only attain relatively small equilibrium velocity dispersion. As a result the most massive protoplanetary embryos can access only those building blocks within their gravitational feeding zones (Kokubo & Ida 1998). When these embryos have collected all the planetesimals within about five times their Roche radius on either side of their orbits, their growth stalls. This maximum embryo mass, a function of planetesimal surface density

and distance from the central star, is referred to as the embryo's isolation mass ($M_{\rm iso}$). Gas giants can only form if the embryos' $M_{\rm iso}$ is sufficiently large for the cores to begin accreting gas prior to the depletion of their nascent disks (Ida & Lin 2004).

Although the gravity of lunar-mass embryos is adequate to accrete disk gas with temperature $< 10^3$ K, *efficient* dynamical gas accretion is only possible for cores with masses greater than some critical value ($M_{\rm crit}$). In a minimum mass solar nebula (Hayashi 1981) with an interstellar grain size distribution, $M_{\rm crit} \sim 10 M_\oplus$ at a semi-major axis $a \sim 5$ AU (Pollack et al. 1996), although this critical mass decreases both with lowered grain opacity (Ikoma et al. 2000; Hubickyj et al. 2005) and with increased density of the ambient gas (Bodenheimer & Pollack 1986; Papaloizou & Terquem 1999). Gas giant formation therefore requires that the heavy-elements in the disk can be efficiently assembled into massive cores with mass greater than $M_{\rm crit}$. In order to understand the spatial distribution of the gas giant planets we must understand how the building blocks of these cores migrate and are retained in gaseous disks.

In protoplanetary disks solid retention first becomes an issue once grains grow beyond a few cm in size. In most regions of protostellar disks, the midplane pressure ($P_{\rm mid}$) decreases with distance from the central star ($r$) so that the gas is slightly pressure supported, resulting in a sub-Keplerian azimuthal velocity. Grains larger than a few cm are decoupled from the gas and move at Keplerian speeds. Consequently, grains typically experience head winds and undergo orbital decay (Weidenschilling 1977). However if $P_{\rm mid}$ does not monotonically decrease with $r$ then immediately interior to a local pressure maximum the gas attains super-Keplerian velocities. This motion introduces a tail wind on the decoupled grains and causes them to drift outwards towards local pressure maxima (Bryden et al. 2000; Haghighipour & Boss 2003).

Solid retention again becomes an issue once planetesimals grow into earth-mass embryos and tidal interactions with the gaseous disk become important. Before embryos are sufficiently massive to open up gaps in the disks (Lin & Papaloizou 1986), they can exchange angular momentum with the gas via their Lindblad and co-rotation resonances (Goldreich & Tremaine 1980). A geometric bias causes an imbalance between the Lindblad resonances which generally leads to a loss of angular momentum and orbital decay for the embryos (Ward 1986, 1997). However, embryos will gain angular momentum through their co-rotation resonances if there is a positive $P_{\rm mid}$ gradient (Tanaka et al. 2002; Masset et al. 2006). Numerical models which take into account these physical effects have reproduced the observed $M_p - a$ distribution around solar type stars (Ida & Lin 2008).

Several physical processes can lead to local maxima in $P_{\rm mid}$. Various authors have explored the potential accumulation of grains at transient pressure maxima formed by tur-

bulent fluctuations (Johansen et al. 2006; Fromang & Nelson 2005) or spiral waves (Rice et al. 2006). These mechanisms, while likely extremely important for forming planetesimals at a large range of radii, are still quite "leaky" as a significant fraction of the solid material simply undergoes a slightly slower random walk towards the central star. However, longer lived pressure maxima may also exist due to large scale changes in the disk viscosity (Kretke & Lin 2007).

We expect radial variations in viscosity if turbulence caused by the magneto-rotational instability (MRI; Balbus & Hawley (1991)) is the primary mechanism for transporting angular momentum. These variations result from changes in the ionization fraction at different radii in the disk since free electrons are needed to couple the gas to the magnetic field. The disk is thermally ionized in the hot inner regions, but further out stellar x-rays and diffuse cosmic rays ionize only the surface layers, resulting in a viscously active turbulent surface sandwiching an inactive "dead zone" (Gammie 1996). At the critical radius marking the inner edge of the dead zone ($a_{\rm crit}$), the effective viscosity decreases with increasing distance from the central star. In a quasi-steady state situation (expected to develop rapidly in the inner regions of the disk) this decrease in viscosity leads to a local increase in the magnitude of $\Sigma_g$ and hence of $P_{\rm mid}$ with radius. This disk structure provides a promising barrier to the orbital decay of both boulders and embryos. The radial location of $a_{\rm crit}$ depends on the stellar mass and the mass accretion rate which we argue explains the observed differences between the statistical distributions of planets around solar-type stars and around intermediate mass stars.

In this paper, we present a model for the formation of planets at the inner edge of the dead zone and argue why this process is more relevant for intermediate mass than for solar mass stars. In §2 we describe our quantitative numerical model for the evolution of solids in the disk, based upon the work of Garaud (2007). An important aspect of this model is the location of $a_{\rm crit}$ (the inner edge of the dead zone) which we derive in §2.2 as a function of stellar mass and mass accretion rate. In §3 we present the model results for a 2 $M_\odot$ star and estimate how this planet formation mechanism scales with stellar mass. In §4 we summarize our conclusions.

## 2. Model Description

In order to assess the probability of forming of gas giants at the inner edge of the dead zone, we must calculate the expected isolation mass of the cores ($M_{\rm iso}$) at this location ($a_{\rm crit}$). From the work of Kokubo & Ida (1998), it has been established that the embryo's isolation mass is sensitive both to the distance from the host star and to the surface density

of solids. For the purpose of computing the efficiency of solid retention we calculate the dynamical evolution of the solids in the disk using a modification of the numerical scheme developed by Garaud (2007) (hereafter G07). For full details we refer the readers to G07 but for reference the salient points are described here. In this model we assume that particles, as a result of a collisional cascade, maintain a power-law size distribution in which the number density of particles of size $s$ goes as $dn/ds \propto s^{-3.5}$, with sizes ranging from a fixed $s_{\rm min}$ to $s_{\rm max}$ and where $s_{\rm max}$ is allowed to vary with time and distance from the central star. This simplifying assumption allows us to completely describe the evolution of the gas and solids in the disk by the total gas surface density ($\Sigma_g(r,t)$), the solid and vapor surface densities of the different species in the disk ($\Sigma_{p,i}(r,t)$ and $\Sigma_{v,i}(r,t)$ respectively), and the maximum size of the particles $s_{\rm max}(r,t)$.

In the following sections we describe how we have modified the G07 scheme. In §2.1, we describe how we account for the presence of an evolving dead zone. In particular we describe in §2.2 how we calculate the location of the inner edge of the dead zone ($a_{\rm crit}$) using a simple model of the vertical thermal structure. Finally, in §2.3 we model the drag on the gas caused by the particles in the limit of large $Z = \Sigma_p/\Sigma_g$, an effect important near $a_{\rm crit}$ where solids are seen to accumulate.

### 2.1. Viscosity at a function of $r$ and $t$

The original G07 model uses the standard $\alpha$ viscosity prescription ($\nu(r) = \alpha_{\rm eff} c_s(r) h(r)$) where $c_s$ is the midplane sound-speed, $h$ is the disk scale-height ($h \equiv c_{s,\rm mid}\Omega_{\rm K}^{-1}$) and $\alpha_{\rm eff}$ is constant. In this paper we consider $\alpha_{\rm eff} = \alpha_{\rm eff}(r,t)$ to model the presence of an evolving MRI-dead zone. In fully MRI-active regions (eg. interior to $a_{\rm crit}$) we assume that $\alpha_{\rm eff} = \alpha_{\rm MRI}$, while exterior to $a_{\rm crit}$, $\alpha_{\rm eff}$ is modified to take into account the lower viscosity of the dead zone. In §2.2 we describe in detail how we calculate the location of $a_{\rm crit}$.

Exterior to $a_{\rm crit}$ the disk is ionized by x-rays and cosmic rays, so only the surface layers are MRI active. The column density of this active layer ($\Sigma_A$) is strongly dependent on the ionizing source (ie. the ability of cosmic rays to penetrate the stellar magnetosphere) and on the recombination rate, which is dominated by the amount of small grains. Due to these uncertainties, and the fact that the exact evolution of the outer parts of the dead zone are relatively unimportant in these calculations, we follow previous studies and assume that $\Sigma_A = 100$ g cm$^{-2}$ at all radii (outside of the thermally ionized region) (eg. Gammie (1996)).

Additionally, we assume that there is some amount of angular momentum transport in the dead zone. This transport may be due to the propagation of MRI-driven waves into

the laminar dead zone (Fleming & Stone (2003); Turner et al. (2007)) or to a mechanism unrelated to the MRI. This motivates the following prescription in regions beyond $a_{\rm crit}$

$$\alpha_{\rm eff}(r,t) = \begin{cases} \frac{2\alpha_{\rm MRI}\Sigma_A + \alpha_{\rm eff,dead}(\Sigma_g - 2\Sigma_A)}{\Sigma_g(r,t)}, & \text{if } \Sigma_g \geq 2\Sigma_A, \\ \alpha_{\rm MRI}, & \text{otherwise,} \end{cases} \tag{1}$$

where $\alpha_{\rm eff,dead}$ is the effective viscosity in the dead zone.

### 2.2. Location of $a_{\rm crit}$

As the degree of thermal ionization is a sensitive function of temperature, we must calculate the vertical structure of the disk in order to find the location of $a_{\rm crit}$, the inner edge of the dead zone. In the innermost regions of the disk viscous heating dominates the energy budget, and stellar irradiation can be neglected (Garaud & Lin 2007).

We assume that the disk is in hydrostatic equilibrium

$$\frac{dP}{dz} = -\rho_g \Omega_K^2 z, \tag{2}$$

and is viscously heated so that the vertical energy flux ($F$) is described by

$$\frac{dF}{dz} = \frac{9}{4}\nu\rho_g\Omega_K^2. \tag{3}$$

Here we consider that $\nu(r,z)$ is a function of both height and radius in the disk and assume that the orbital frequency can be approximated by the Keplerian frequency.

We also assume radiative energy transport so that

$$F = -\frac{4ac}{3}\frac{T^3}{\kappa\rho_g}\frac{dT}{dz}, \tag{4}$$

where $\kappa$ is the Rosseland mean opacity. For the temperature range of interest (400-1,200K) the dominant opacity sources are silicate and iron grains. We adopt a grey opacity approximation in which $\kappa = 1$ cm$^2$ g$^{-1}$. This approximation is consistent with the Ferguson et al. (2005) dust opacities. We solve only the optically thick region of the disk and use photospheric boundary conditions at $z = z_e$, namely $P(z_e) = (2/3)\Omega_K^2 z_e/\kappa$ and $F(z_e) = \sigma T(z_e)^4$. Finally we assume symmetry about the midplane.

In order to parametrize the variation of the viscosity with height above the midplane we follow the results of 3D MHD simulations which demonstrate that, in fully developed MRI-turbulence, the shear stress($w \equiv \nu\rho_g r(d\Omega/dr) = (3/2)\nu\rho_g\Omega_{\rm K}$) is approximately constant

with height (Miller & Stone 2000). Based on these numerical results, we model the viscosity at a given radius as

$$\nu(z) = \begin{cases} \frac{2}{3}\frac{\alpha P_{\rm mid}}{\rho_g(z)\Omega_{\rm K}}, & \text{if } |z| < z_\nu, \\ 0, & \text{otherwise,} \end{cases} \tag{5}$$

where $z_\nu \approx 2h$. Note that this differs from the more common 2D parametrization sometime referred to as the "$\alpha P$-formalism" (e.g. Cannizzo (1992)) where $\nu_{\alpha-P} = \alpha c_s^2(z)\Omega_{\rm K}^{-1}$. Viscosity described by equation (5) increases with height, which leads to a cooler midplane more consistent with multi-dimensional MHD simulations than the $\alpha P$-formalism (Hirose et al. 2006).

Equation (5) is applicable to MRI-active regions where the partially ionized gas is well coupled to the turbulent magnetic field through the entire thickness of the disk. As long as the midplane temperature is high enough to sufficiently ionize the gas this structure is self-consistent. We can therefore use it to determine $a_{\rm crit}$, the outermost radius where this condition is satisfied. In practice we combine the equations for the vertical structure with the Saha equation to calculate the location at which the midplane just satisfies the ionization criteria of $x_e \geq 10^{-12}$ (where $x_e$ is the fractional number density of electrons) which corresponds to $T \sim 1000$K for typical disk midplane densities (Umebayashi 1983).

In Figure 2 the curves show the location of the inner edge of the dead zone as a function of stellar mass and accretion rate assuming that in the active region $\alpha = 10^{-2}$. These theoretical curves can be approximated by

$$\begin{aligned} a_{\rm crit} &= 0.77 \left(\frac{\dot{M}}{1.4\times10^{-7} M_\odot {\rm yr}^{-1}}\right)^{4/9} \left(\frac{M_*}{2M_\odot}\right)^{1/3} \\ &\quad \times \left(\frac{\alpha}{10^{-2}}\right)^{-1/5} \left(\frac{\kappa_D}{1\ {\rm cm}^2\ {\rm g}^{-1}}\right)^{1/4} {\rm AU}, \end{aligned} \tag{6}$$

where the quasi-steady-state approximation for the mass accretion rate

$$\dot{M} = 3\pi \int_{-\infty}^{\infty} \rho_g \nu dz = 4\pi\alpha P_{\rm mid}\Omega_{\rm K}^{-1} z_\nu \tag{7}$$

was used to eliminate $P_{\rm mid}$. We find that this value for $a_{\rm crit}$ varies significantly from the $\sim 0.1$ AU often quoted (ie. Gammie (1996)) if the stellar mass or the mass accretion rate are large. By using the relationship

$$\dot{M} = 3\pi\nu\Sigma_g = 3\pi\alpha_{\rm eff} c_s^2 \Omega_{\rm K}^{-1}\Sigma_g \tag{8}$$

(Pringle 1981) we can relate the $\alpha$ in equation (6) to the the vertically averaged $\alpha_{\rm eff}$ when the disk is fully MRI active and find that $\alpha_{\rm MRI} \approx \alpha$.

Observationally, $\dot{M}$ appears to be correlated with $M_*$, although the exact relationship is both uncertain and shows significant scatter. For reference the symbols in Figure 2 indicate measurements of mass accretion rates onto young stars. The solid points are from observations of the young cluster ($< 1$ Myr) $\rho$-Oph by Natta et al. (2006) and the dashed line shows the best fit to their data which is

$$\dot{M} \simeq 4 \times 10^{-8} (M_*/M_\odot)^{1.8} M_\odot \mathrm{yr}^{-1}. \tag{9}$$

As the mass accretion rate for the higher mass stars in the Natta et al. sample is dominated by a single object, we have also plotted (as open points) similar data from older, heterogeneously distributed intermediate mass stars with estimated ages ranging from 1-10 Myr (Garcia Lopez et al. 2006). As suggested in this study, these systematically older stars may have had higher mass accretion rates consistent with the extrapolation from $\rho$-Oph, when they were younger.

Using the best fit relationship from $\rho$-Oph implies that $a_{\rm crit} \propto M_*^{1.1}$. Clarke & Pringle (2006) suggest that the correlation between stellar mass and mass accretion rate may not be this steep due to observational biases. If instead we use their estimation that $\dot{M} \propto M_*$, then $a_{\rm crit} \propto M_*^{0.8}$, which is a slightly less sensitive but nevertheless increasing function of $M_*$. Therefore, in the light of these the uncertainties, we will simply assume that $a_{\rm crit} \propto M_*$.

### 2.3. Gas-Particle Feedback

In a thin disk, the global evolution of the gas surface density $\Sigma_g$ is determined by the equation

$$\frac{\partial \Sigma_g}{\partial t} + \frac{1}{r}\frac{\partial}{\partial r}\left(\Sigma_g u_r r\right) = 0. \tag{10}$$

In a standard viscous accretion disk the radial velocity ($u_r$) of gas equals $u_\nu$ where

$$u_\nu \equiv -\frac{3}{r^{1/2}\Sigma_g}\frac{\partial}{\partial r}(r^{1/2}\nu\Sigma_g). \tag{11}$$

In our analysis, we consider the possibility that the radial velocity of the gas $u_r$ is not only determined by the viscosity but also by momentum transferred via drag between the gas and the solid particles. We calculate the equation of motion for a parcel of gas and dust in a similar fashion to Nakagawa et al. (1986). However, instead of assuming a single particle size for the solids we consider the power-law distribution ($dn/ds \propto s^{-3.5}$). The equation of motion for a given particle of size $s$ is

$$\frac{d\boldsymbol{V}(s)}{dt} = -\frac{1}{\tau_s(s)}(\boldsymbol{V}(s) - \boldsymbol{U}) - \frac{GM_*}{r^3}\boldsymbol{r} \tag{12}$$

where $\tau_s(s) = s\rho_s/(\rho_g c_s)$ is the stopping time for a particle of size $s$ and density $\rho_s$ (in the Epstein regime, see G07 for a full description), where $\boldsymbol{V}(s)$ is the size dependent particle velocity and $\boldsymbol{U}$ is the gas velocity.

Assuming that deviations from Keplerian orbital velocity are small, we write $\boldsymbol{V}(s) = v_r(s)\hat{r} + (r\Omega_{\rm K} + v_\phi(s))\hat{\boldsymbol{\phi}}$ and $\boldsymbol{U} = u_r\hat{r} + (r\Omega_{\rm K} + u_\phi)\hat{\boldsymbol{\phi}}$). The linearization of equation (12) yields

$$\begin{aligned}\frac{\partial v_r}{\partial t} &= -\frac{1}{\tau_s(s)}(v_r(s) - u_r) + 2\Omega_{\rm K} v_\phi(s), \\ \frac{\partial v_\phi}{\partial t} &= -\frac{1}{\tau_s(s)}(v_\phi(s) - u_\phi) - \frac{1}{2}\Omega_{\rm K} v_r(s),\end{aligned} \tag{13}$$

The particles and gas adjust to a steady motion with respect to each other within a few stopping times, so we solve for the steady-state solutions only. Multiplying by the particle mass and integrating over the whole size distribution function yields

$$\begin{aligned}\int_{s_{\rm min}}^{s_{\rm max}} \left[-m(s)\frac{dn}{ds}\frac{1}{\tau_s(s)}(v_r(s) - u_r) + 2\Omega_{\rm K} m(s)\frac{dn}{ds}v_\phi(s)\right] ds &= 0, \\ \int_{s_{\rm min}}^{s_{\rm max}} \left[-m(s)\frac{dn}{ds}\frac{1}{\tau_s(s)}(v_\phi(s) - u_\phi) - \frac{1}{2}\Omega_{\rm K} m(s)\frac{dn}{ds}v_r(s)\right] ds &= 0.\end{aligned} \tag{14}$$

The momentum lost by the solids is acquired by the gas, so that the steady state gas-dynamic can be described by

$$\begin{aligned}\int_{s_{\rm min}}^{s_{\rm max}} m(s)\frac{dn}{ds}\frac{1}{\tau_s(s)}(v_r(s) - u_r)ds + 2\Omega_{\rm K}\rho_g(u_\phi + \eta v_K) &= 0, \\ \int_{s_{\rm min}}^{s_{\rm max}} m(s)\frac{dn}{ds}\frac{1}{\tau_s(s)}(v_\phi(s) - u_\phi)ds - \frac{1}{2}\Omega_{\rm K}\rho_g(u_r - u_\nu) &= 0,\end{aligned} \tag{15}$$

where $\eta$ is the non-dimensional pressure gradient

$$\eta \equiv -\frac{1}{2}\frac{h^2}{r^2}\frac{\partial \ln P}{\partial \ln r}, \tag{16}$$

and $v_K = r\Omega_{\rm K}$. In most regions of the disk $\eta$ is positive due to the negative pressure gradient, but its sign will change around pressure maxima. In the absence of particles, the gas will have an azimuthal velocity (relative to the Keplerian motion) of $u_\phi = -\eta v_K$ and a radial velocity of $u_r = u_\nu$.

Combining these equations and defining the mass–weighted average particle velocities as

$$\begin{aligned}\bar{v}_\phi &\equiv \frac{1}{\rho_p}\int_{s_{\rm min}}^{s_{\rm max}} m(s)\frac{dn}{ds}v_\phi(s)ds, \\ \bar{v}_r &\equiv \frac{1}{\rho_p}\int_{s_{\rm min}}^{s_{\rm max}} m(s)\frac{dn}{ds}v_r(s)ds\end{aligned} \tag{17}$$

allows us to write

$$\begin{aligned} u_\phi &= -\frac{\rho_p}{\rho_g}\bar{v}_\phi, \\ u_r &= u_\nu - \frac{\rho_p}{\rho_g}\bar{v}_r. \end{aligned} \tag{18}$$

Combining this with equation (13) we can solve for

$$\begin{aligned} v_r(s) &= \frac{u_r + 2\Omega_{\rm K}\tau_s(s)u_\phi}{1+\Omega_{\rm K}^2\tau_s(s)^2}, \\ v_\phi(s) &= \frac{u_\phi - (1/2)\Omega_{\rm K}\tau_s(s)u_r}{1+\Omega_{\rm K}^2\tau_s(s)^2}. \end{aligned} \tag{19}$$

Using the definition for the Stokes number $\mathrm{St}(s) = \Omega_{\rm K}\tau_s(s)/(2\pi)$ and taking the mass–weighted integral over all particle sizes yields

$$\begin{aligned} \bar{v}_r &= I\left(\sqrt{2\pi\mathrm{St}_{\rm max}}\right)u_r + 2J\left(\sqrt{2\pi\mathrm{St}_{\rm max}}\right)u_\phi, \\ \bar{v}_\phi &= I\left(\sqrt{2\pi\mathrm{St}_{\rm max}}\right)u_\phi - \frac{1}{2}J\left(\sqrt{2\pi\mathrm{St}_{\rm max}}\right)u_r, \end{aligned} \tag{20}$$

where $I$ and $J$ are the same as equation (52) in G07 (reproduced in Appendix A for reference) and $\mathrm{St}_{\rm max} = \mathrm{St}(s_{\rm max})$. Combining equations (18) and (20) yields the final steady-state velocities for the particles and the gas where $I \equiv I\left(\sqrt{2\pi\mathrm{St}_{\rm max}}\right)$, $J \equiv J\left(\sqrt{2\pi\mathrm{St}_{\rm max}}\right)$, and $\chi \equiv \rho_p/\rho_g$.

$$\begin{aligned} \bar{v}_r &= \frac{[I+\chi(I^2+J^2)]u_\nu - 2J\eta v_K}{1+2\chi I+\chi^2(I^2+J^2)}, \\ \bar{v}_\phi &= -\frac{1}{2}\left[\frac{Ju_\nu + 2[I+\chi(I^2+J^2)]\eta v_K}{1+2\chi I+\chi^2(I^2+J^2)}\right], \end{aligned} \tag{21}$$

$$\begin{aligned} u_r &= \frac{(1+\chi I)u_\nu + 2J\chi\eta v_K}{1+2\chi I+\chi^2(I^2+J^2)}, \text{ and} \\ u_\phi &= \frac{1}{2}\left[\frac{\chi J u_\nu - 2(1+\chi I)\eta v_K}{1+2\chi I+\chi^2(I^2+J^2)}\right]. \end{aligned} \tag{22}$$

In the gas dominated limit ($\chi \to 0$) these equations reduce to those in G07. If $\mathrm{St}_{\rm max}$ is large and $\mathrm{St}_{\rm max} \gg \chi^2$, the solids will be decoupled from the gas and will not migrate significantly ($v_r = 0$) while the gas evolves viscously ($u_r = u_\nu$). In the limit $\mathrm{St}_{\rm max} \ll 1$, the grains are well-coupled to the gas so there will be little relative motion between the two ($u_r = v_r = u_\nu/(1+\chi)$).

## 3. Model Results

With these modifications to the G07 prescription we calculate the evolution of a disk around a $2M_{\odot}$ star including an MRI-dead zone ($\alpha_{\rm MRI} = 10^{-2}$, $\alpha_{\rm eff,dead} = 10^{-3}$). The initial disk has a surface density profile of

$$\Sigma_g = \Sigma_0 \left(\frac{r}{1\rm AU}\right)^{-1} \exp\left(\frac{-r}{R_0}\right) \tag{23}$$

where $R_0 = 30$AU, and $\Sigma_0 = 10^4$ g cm$^{-2}$ has been chosen such that the quasi-steady state accretion rate $\dot{M}$ from equation (8) is $1.4 \times 10^{-7}\dot{M}$ yr$^{-1}$ when $\alpha_{\rm eff} = \alpha_{\rm eff,dead}$. For the chosen value of $\alpha_{\rm eff,dead}$ the total disk mass is $0.1M_*$. This relatively massive disk is still stable according to the Toomre criterion at all radii. For simplicity we only track one species of solids, a generic refractory material which we take to be a combination of silicates and metals, materials which are assumed to sublimate at 1500K. Using the solar composition from Lodders (2003) we begin with a dust-to-gas ratio of 0.005 for these refractory materials. We do not track volatile ices as they will not contribute to the solid cores formed in the hot regions of interest. For other model parameters we use the values presented in the fiducial model of G07.

### 3.1. Accumulation of Solids

We first study the accumulation of solids near the edge of the dead zone and emphasize the importance of feedback in terms of momentum exchange between the solids and the gas. We present two runs, the first neglecting momentum transfer from the dust to the gas and then including this feedback.

The top and middle panels of figure 3 show the evolution of the gas and solids neglecting the feedback of the dust on the gas. For reference, figure 4 shows $\alpha_{\rm eff}$ at $10^4$ years and at $10^5$ years to indicate the location of the dead zone. Early on the dead zone extends from 0.9 to 20 AU, but as the disk evolves the dead zone shrinks. Within the first $10^4$ years the gaseous disk adjusts to a quasi-steady-state profile in the inner regions. The surface density of the gas in the fully MRI-active inner region ($r \lesssim 1$ AU) is reduced by a factor of $\alpha_{\rm eff,dead}/\alpha_{\rm MRI}$ compared with that in the dead zone ($r \in [1, 10]$ AU), thus creating a local pressure maximum near 1 AU. In this calculation neglecting feedback, the solids accumulate in a very narrow ring corresponding to this pressure maximum. After only $5.3 \times 10^5$ years the largest-size body at this location reaches $5M_{\oplus}$ and the core thus formed is expected to continue to grow significantly due to accretion of gas, not included in this numerical calculation. Crucially, in this model tidal interactions will not affect the orbital evolution of the core as the effect of

Type I migration would be to keep the core at the pressure maximum (Masset et al. 2006). It is also interesting to note that when feedback is neglected, virtually all solids are trapped at the pressure maximum and negligible amounts of heavy elements accrete onto the star. This effect is associated with the clear spatial separation of the pressure maximum and the sublimation line (here at $\sim 0.3$ AU) and would appear to predict that intermediate-mass stars should be strongly depleted in refractory elements. However we now show that this is in fact unrealistic as the large build up of material makes it necessary to include the transfer of momentum from the solids to the gas.

The bottom panels of figure 3 show the evolution of the same initial disk including this momentum feedback. The early evolution is essentially similar for $t < 10^4$ yrs. However, once the amount of solids in the inner edge of the dead zone has increased by an order of magnitude, it begins affecting the gas properties (compare the middle and bottom panels of fig 3). The mass accretion rate onto the star decreases as the gas receives angular momentum from the solids. The decrease in $\dot{M}$ reduces the surface density and thus the midplane temperature, causing $a_{\rm crit}$ to move inwards. As $a_{\rm crit}$ moves inwards the particles of different sizes respond to this shift in location at different rates, smoothing the sharp peak in the solid surface density and allowing the trapped gasses to accrete onto the central star. In this way both $\dot{M}$ and the position of $a_{\rm crit}$ oscillate with time as seen in figure 5. It is also interesting to note that these oscillations allow heavy elements to accrete onto the star since when $a_{\rm crit}$ moves outwards it leaves some solids interior to the "trap" of the pressure maximum. Thus intermediate-mass stars will not, in fact, be significantly depleted in refractory elements. In these simulations we find that the total amount of solids trapped near the pressure maximum is of the order of 100 $M_\oplus$ and that the dust-to-gas ratio in this region is of order unity. The core growth is slower than in the simulation without feedback as material is deposited over a wider range of radii. In $5.3 \times 10^5$ yrs the largest body has grown to $0.5 M_\oplus$ but the amount of material in its vicinity suggests that it will continue to grow larger still.

### 3.2. Core Formation

As the core mass increases much beyond 0.5 $M_\oplus$ many effects not included in the numerical algorithm could affect its growth. For example, it may be important to include the effects of tidal interactions since the oscillations of the position of the pressure maximum could affect the orbital evolution of the core. Additionally, gravitational interactions between solids may start to impact their radial distribution. The cores may scatter each other out of the region of interest and radially migrating solids will be trapped into resonances with the existing core, stalling radial migration (Weidenschilling & Davis 1985). As a result,

we do not continue integrating the simulations beyond this point but instead estimate the achievable core mass with simpler but robust scalings based on our most important results from the previous section: (1) the presence of a large reservoir of solids ($> 100 M_\oplus$) around $a_{\rm crit}$ and (2) the saturation of the dust-to-gas surface density ratio to $Z \sim 1$ near $a_{\rm crit}$ (as seen in fig. 3), which is a simple consequence of the saturation of the nonlinear momentum feedback between the solids and the gas.

Using these ideas, we estimate the *maximum* achievable core size from the isolation mass (Ida & Lin 2005) at $a_{\rm crit}$ is

$$M_{\rm iso} = 2\pi \Sigma_p a_{\rm crit} b r_H(a_{\rm crit}), \tag{24}$$

where $r_H(a_{\rm crit}) = a_{\rm crit}(2M_{\rm iso}/(3M_*))^{1/3}$ is the Hill's radius and $b \simeq 10$ (Lissauer 1987). We assume that $\Sigma_g$ is related to $\dot{M}$ by the quasi-steady-state approximation (8), and that $\Sigma_p$ is related to the gas density via $Z = \Sigma_p/\Sigma_g$ where $Z \sim 1$. We find that

$$\begin{aligned} M_{\rm iso} &\simeq 60\ Z^{3/2} \left( \frac{\dot{M}}{1.4 \times 10^{-7} M_\odot {\rm yr}} \right)^{11/6} \\ &\times \left( \frac{M_*}{M_\odot} \right)^{1/2} \left( \frac{T}{10^3 K} \right)^{-3/2} \left( \frac{\alpha_{\rm MRI}}{10^{-2}} \right)^{-4/3}\ M_\oplus. \end{aligned} \tag{25}$$

Note that this estimate should be considered as a maximum achievable size and that, more realistically, cores may only reach a fraction of $M_{\rm iso}$. Therefore in the following section we select the core mass $M_c = f M_{\rm iso}$. The isolation mass of the core at $a_{\rm crit}$ goes as $M_{\rm iso} \propto \dot{M}^{11/6} M_*^{1/2}$. If we assume that $\dot{M}$ is related to $M_*$ as discussed in §2.2 then $M_{\rm iso} \propto M_*^2$ to $M_*^4$. Therefore, super-earth cores form preferentially at the inner boundary of the dead zone around more massive stars.

### 3.3. Gas Giant Formation

As our numerical algorithm does not include gas accretion onto the cores we can use the estimate of core mass derived in the previous section to look at the potential for further growth using the approximations of Ida & Lin (2005). The growth of a planet of mass $M_p$ due to the gas capture can be approximated as

$$\frac{dM_p}{dt} \approx \frac{M_p}{\tau} \tag{26}$$

where

$$\tau \approx \tau_0 \left( \frac{M_p}{M_\oplus} \right)^{-3} \tag{27}$$

with $\tau_0 \approx 10^{10}$ years (see Ida & Lin (2005), although $\tau_0$ is likely to be smaller in the inner regions of the disk where $\rho_g$ is relatively large). As long at the final mass of the planet is much greater than the original core mass, the timescale for giant planet formation is then

$$t_{\rm giant} \approx \frac{\tau_0}{3} \left( \frac{M_c}{M_\oplus} \right)^{-3}. \tag{28}$$

This inference effectively means that in order for a gas giant to form within the lifetime of the evolving disk, the core mass must at least be of the order of 10 $M_\oplus$. Using the relationship derived in equation (25) implies that $t_{\rm giant} \propto \dot{M}^{-11/2} M_*^{-3/2}$. Folding in the relationship between $\dot{M}$ and $M_*$ yields $t_{\rm giant} \propto M_*^{-7}$ to $M_*^{-12}$. This very steep function demonstrates that giant planets will not have time to form at the inner edge of the dead zone around less massive stars, but will form ubiquitously around higher mass stars with higher accretion rates.

### 3.4. Asymptotic Mass and Multiple Planet Systems

The observationally inferred mass of the known planets around stars with $M_* > 2M_\odot$ is in the range of $2 - 20 M_J$ which is near the upper end of the $M_p$ distribution of known planets around solar-type stars. In the core-accretion scenario, the asymptotic mass of gas giants is determined by a thermal truncation condition (Lin & Papaloizou 1993) such that

$$M_p \simeq f_a (h/r)^3 M_*, \tag{29}$$

where the constant $f_a$ is of the order of 1 to 10 and depends on the detailed thermal structure of the disk (Dobbs-Dixon et al. 2007; Ida & Lin 2005). We use equation (6) to determine the value of $h/r = c_s/v_K$ at $a_{\rm crit}$. The temperature and sound speed at the inner edge of partially dead zone is, by construction, independent of $M_*$ and $\dot{M}$. We find from equations (6) and (9) that, at $a_{\rm crit}$, $h/r \sim 0.05$ during the main phase of disk evolution. From this result, we estimate that

$$M_p \approx 0.3 f_a \left( \frac{h/r}{0.05} \right)^3 \left( \frac{M_*}{2M_\odot} \right) M_J. \tag{30}$$

Figure 2 shows that the dependence of $\dot{M}$ on $M_*$ in equation (9) is an average relation with considerable dispersion. Furthermore, $\dot{M}$ declines with the stellar age $t_*$. Within our model planets with larger $M_p$ on longer period orbits can form during the early epochs of disk evolution when $\dot{M}$ is much larger and $a_{\rm crit}$ is correspondingly further out. However, the rapid-accretion phase may be too brief for embryos to reach their isolation mass. Nevertheless,

cores with sufficient mass to initiate efficient gas accretion are likely to emerge when $\dot{M}$ is reduced to that approximated by equation (9) and when the timescale for core formation at $a_{\rm crit}$ becomes comparable to the disk evolution timescale. Additionally, due to this spread in $\dot{M}$ around stars with similar $M_*$ we anticipate there will be a wide distribution of planetary masses, albeit the mean value of $M_p$ should vary with $M_*$.

In disks with protracted high-$\dot{M}$ evolution, the first generation of gas giants forms rapidly. Once the first planet has formed and grown large enough to open a gap, the outer edge of this gap provides another pressure maximum capable of trapping solids and promoting the formation of the next planet (Bryden et al. (2000)). We anticipate a prolific production of multiple planetary systems for intermediate-mass stars.

## 4. Summary and Discussion

While planets are likely to form by the same basic mechanisms regardless of the environment in which they form, the properties of their host stars and the detailed structure of their nascent disks will strongly affect the statistical outcome of the formation process. Observations hint that planets may form systematically more efficiently around intermediate mass stars, and that there is a statistically significant lack of giant planets on orbits with semi-major axes much smaller than 1 AU. In this paper we propose a mechanism which forms giant planets preferentially around intermediate mass stars with radial distributions roughly consistent with these observations. In this model the gaseous protoplanetary disk evolves due to MRI-driven turbulence, creating a pressure maximum at the inner edge of the dead zone ($a_{\rm crit}$) which traps solid material. In order for the cores formed at this location to grow large enough to seed giant planets, the inner edge of the dead zone must be sufficiently far from the host star. We demonstrate that, as $a_{\rm crit}$ is roughly proportional to $M_*$, this condition is only likely to be met around intermediate mass stars.

The amount of solids which accumulates near $a_{\rm crit}$ is limited by momentum feedback on the gas by the solids. This is interesting as it means that the surface density of solids at $a_{\rm crit}$ depends on the gas surface density and *not* on the initial fraction of solids, except in extremely metal poor disks. This suggests that while there may be a critical metallicity required in order to form planets by the mechanism described in this paper, beyond that critical value the frequency of giant planets should depend only weakly on stellar metallicity.

The prolific production of gas giants near $a_{\rm crit}$ can also promote the emergence of additional gas giants at larger distances from the same host stars. We may expect the fraction of intermediate-mass stars with multiple Jupiter-mass planets is likely to be larger than that

around solar-type stars. Nevertheless, we anticipate the peak in the planets' semi-major axis distribution to be around 1 AU. This corresponds to the location of the original pressure maximum at the inner edge of the dead zone. Quantitative verification of this expectation requires population synthesis which will be carried out and presented elsewhere. Observational confirmation of this peaked period distribution will provide clues and constraints on the outstanding issue of magnetic turbulent transport in protostellar disks.

ACKNOWLEDGMENTS. We thank D. Fischer, S. Ida, and P. Bodenheimer for many useful conversations. This work is supported by NASA (NAGS5-11779, NNG06-GF45G, NNX07A-L13G, NNX07AI88G), JPL (1270927), and NSF(AST-0507424).

## A. Functions I and J

The functions $I$ and $J$ used in equation (20) and (22) are

$$\begin{aligned} I(x) &= \frac{\sqrt{2}}{4x}[f_1(x) + f_2(x)], \\ J(x) &= \frac{\sqrt{2}}{4x}[-f_1(x) + f_2(x)], \\ f_1(x) &= \frac{1}{2}\ln\left(\frac{x^2 + x\sqrt{2} + 1}{x^2 - x\sqrt{2} + 1}\right), \\ f_2(x) &= \arctan\left(x\sqrt{2} + 1\right) + \arctan\left(x\sqrt{2} - 1\right). \end{aligned} \tag{A1}$$

In the limit of $x \ll 1$, $I = 1$ and $J = x^2/3$, and in the limit of $x \gg 1$, $I = J = \sqrt{2}\pi/(4x) \approx 1/x$.

## REFERENCES

Balbus, S. A., & Hawley, J. F. 1991, ApJ, 376, 214

Bodenheimer, P., & Pollack, J. B. 1986, Icarus, 67, 391

Bryden, G., Różyczka, M., Lin, D. N. C., & Bodenheimer, P. 2000, ApJ, 540, 1091

Cannizzo, J. K. 1992, ApJ, 385, 94

Clarke, C. J., & Pringle, J. E. 2006, MNRAS, 370, L10

Dobbs-Dixon, I., Li, S. L., & Lin, D. N. C. 2007, ApJ, 660, 791

Ferguson, J. W., Alexander, D. R., Allard, F., Barman, T., Bodnarik, J. G., Hauschildt, P. H., Heffner-Wong, A., & Tamanai, A. 2005, ApJ, 623, 585

Fleming, T., & Stone, J. M. 2003, ApJ, 585, 908

Fromang, S., & Nelson, R. P. 2005, MNRAS, 364, L81

Galland, F., Lagrange, A.-M., Udry, S., Beuzit, J.-L., Pepe, F., & Mayor, M. 2006, A&A, 452, 709

Gammie, C. F. 1996, ApJ, 457, 355

Garaud, P. 2007, ApJ, 671, 2091

Garaud, P., & Lin, D. N. C. 2007, ApJ, 654, 606

Garcia Lopez, R., Natta, A., Testi, L., & Habart, E. 2006, A&A, 459, 837

Goldreich, P., & Tremaine, S. 1980, ApJ, 241, 425

Griffin, R. E. M., David, M., & Verschueren, W. 2000, A&AS, 147, 299

Haghighipour, N., & Boss, A. P. 2003, ApJ, 598, 1301

Hayashi, C. 1981, Progress of Theoretical Physics Supplement, 70, 35

Hirose, S., Krolik, J. H., & Stone, J. M. 2006, ApJ, 640, 901

Hubickyj, O., Bodenheimer, P., & Lissauer, J. J. 2005, Icarus, 179, 415

Ida, S., & Lin, D. N. C. 2004, ApJ, 604, 388

—. 2005, ApJ, 626, 1045

—. 2008, ArXiv e-prints, 802

Ikoma, M., Nakazawa, K., & Emori, H. 2000, ApJ, 537, 1013

Johansen, A., Klahr, H., & Henning, T. 2006, ApJ, 636, 1121

Johnson, J. A., Fischer, D. A., Marcy, G. W., Wright, J. T., Driscoll, P., Butler, R. P., Hekker, S., Reffert, S., & Vogt, S. S. 2007, ApJ, 665, 785

Kokubo, E., & Ida, S. 1998, Icarus, 131, 171

Kretke, K. A., & Lin, D. N. C. 2007, ApJ, 664, L55

Lin, D. N. C., & Papaloizou, J. 1986, ApJ, 309, 846

Lin, D. N. C., & Papaloizou, J. C. B. 1993, in Protostars and Planets III, ed. E. H. Levy & J. I. Lunine, 749–835

Lissauer, J. J. 1987, Icarus, 69, 249

Lodders, K. 2003, ApJ, 591, 1220

Lovis, C., & Mayor, M. 2007, A&A, 472, 657

Masset, F. S., Morbidelli, A., Crida, A., & Ferreira, J. 2006, ApJ, 642, 478

Miller, K. A., & Stone, J. M. 2000, ApJ, 534, 398

Nakagawa, Y., Sekiya, M., & Hayashi, C. 1986, Icarus, 67, 375

Natta, A., Testi, L., & Randich, S. 2006, A&A, 452, 245

Papaloizou, J. C. B., & Terquem, C. 1999, ApJ, 521, 823

Pollack, J. B., Hubickyj, O., Bodenheimer, P., Lissauer, J. J., Podolak, M., & Greenzweig, Y. 1996, Icarus, 124, 62

Pringle, J. E. 1981, ARA&A, 19, 137

Rice, W. K. M., Armitage, P. J., Wood, K., & Lodato, G. 2006, MNRAS, 373, 1619

Tanaka, H., Takeuchi, T., & Ward, W. R. 2002, ApJ, 565, 1257

Turner, N. J., Sano, T., & Dziourkevitch, N. 2007, ApJ, 659, 729

Umebayashi, T. 1983, Progress of Theoretical Physics, 69, 480

Ward, W. R. 1986, Icarus, 67, 164

—. 1997, Icarus, 126, 261

Weidenschilling, S. J. 1977, MNRAS, 180, 57

Weidenschilling, S. J., & Davis, D. R. 1985, Icarus, 62, 16

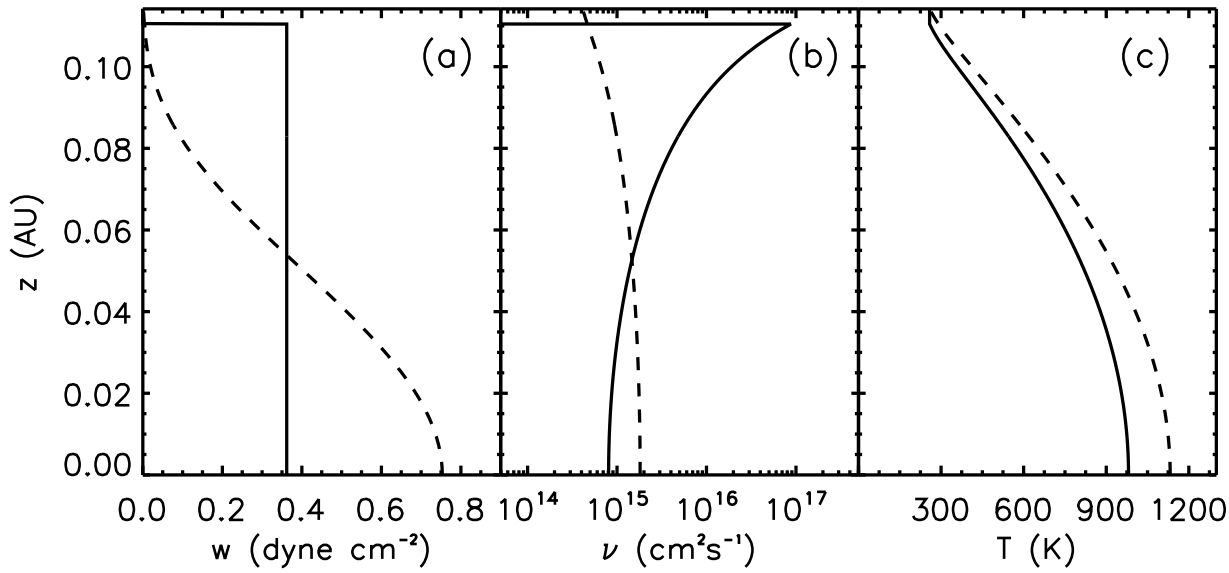


Fig. 1.— A comparison of the disk structure resulting from the viscosity prescription from eq. (5) (solid curves) to disks with the traditional "$\alpha$-P formalism" (dashed curves). The panel (a) shows the accretion stress, panel (b) the viscosity, and panel (c) the temperature.

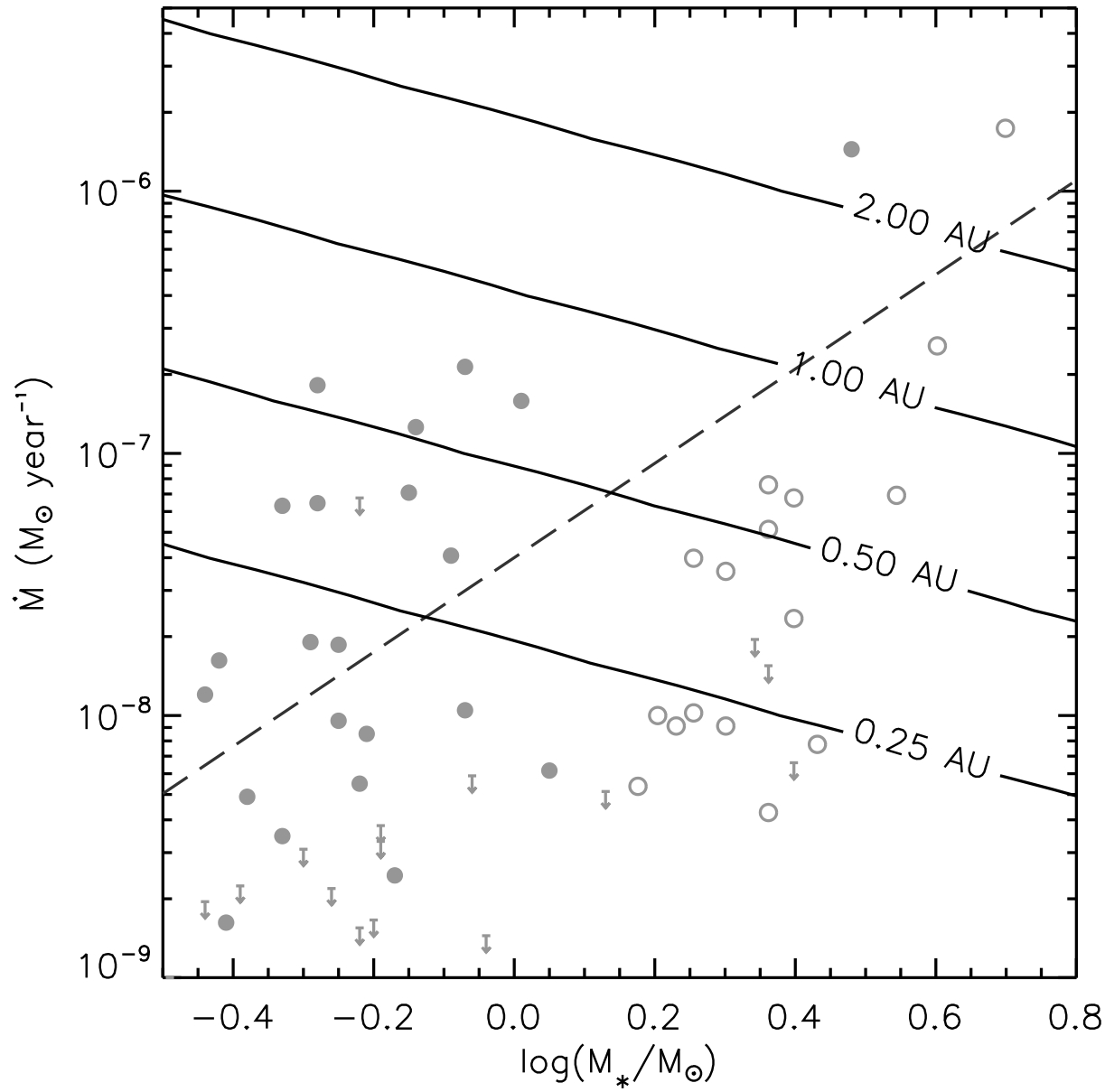


Fig. 2.— The curves show the position of the inner edge of the dead zone as a function of stellar mass and mass accretion rate. Symbols represent observations of mass accretion rates for stars of various masses (see text for details). The dashed line shows the best-fit for the $\rho$-Oph cluster from Natta et al. (2006).

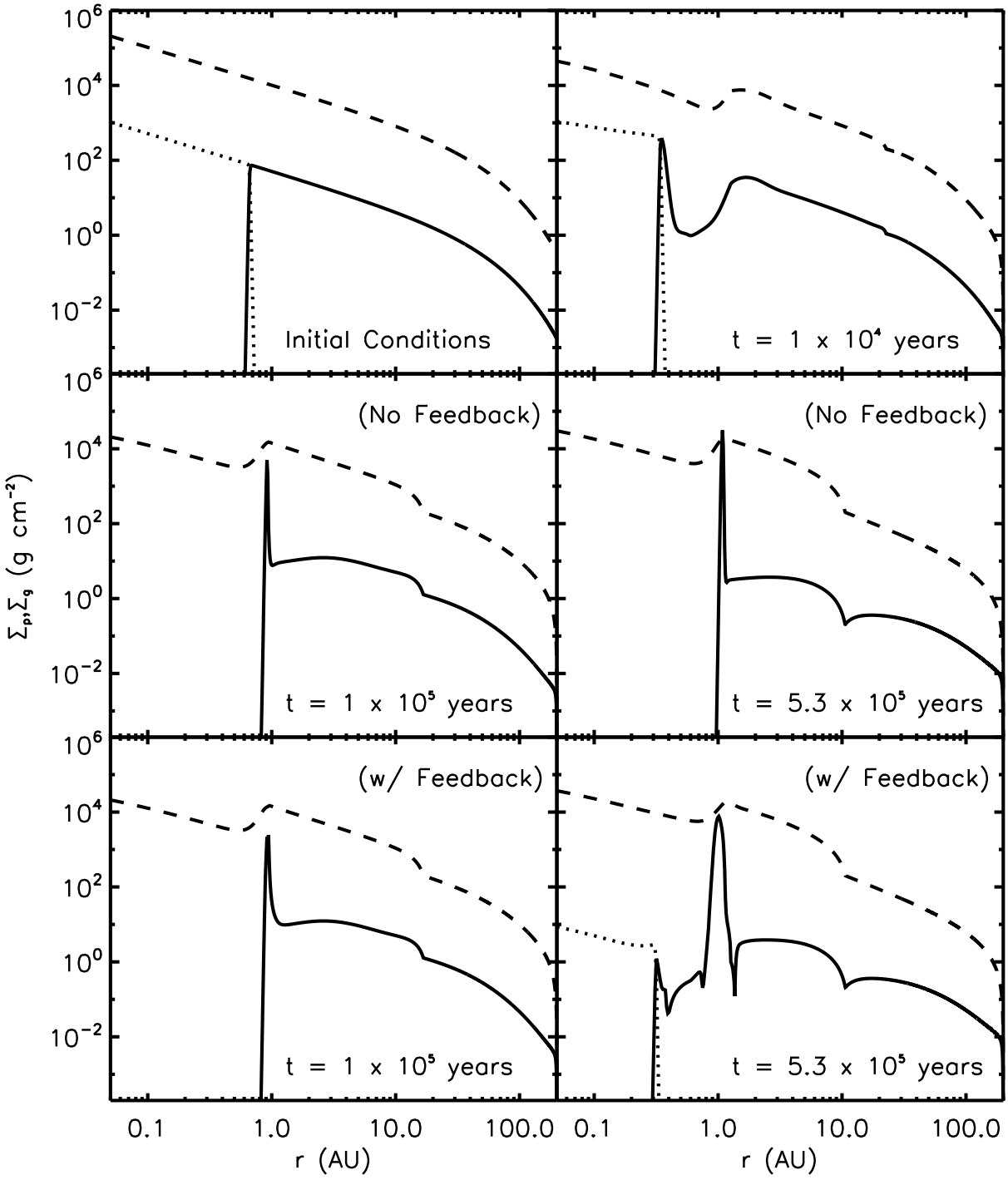


Fig. 3.— Evolution of the surface density of solids (solid curve), gas (dashed curve) and heavy element in vapor form (dotted curve). The middle panels show the evolution neglecting feedback of the dust on the gas while the bottom panels include feedback.

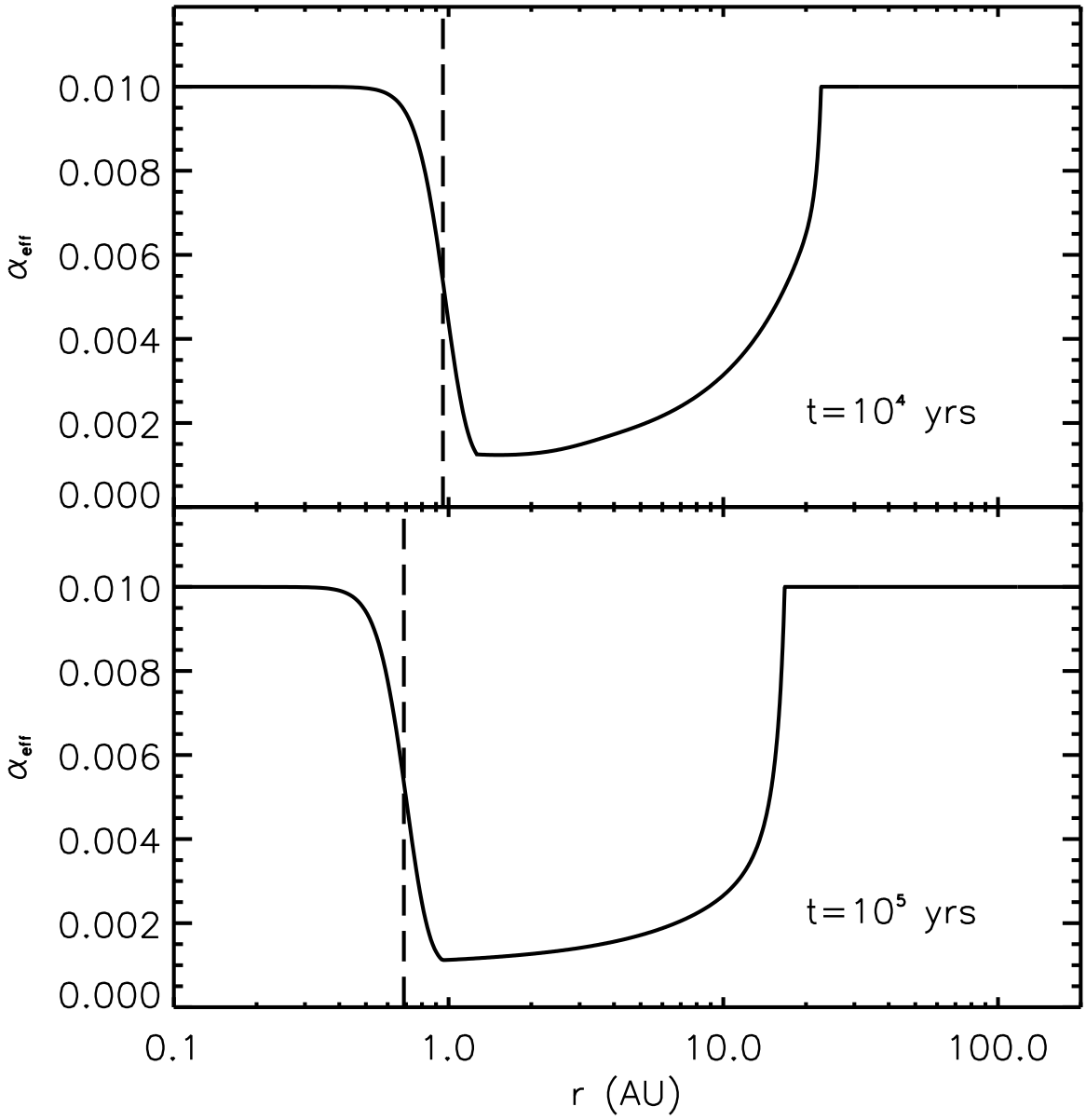


Fig. 4.— The calculated $\alpha_{\rm eff}$ as a function of radius at $10^4$ and $10^5$ years. The inner edge of the dead zone, $a_{\rm crit}$ is indicated by the dotted line.

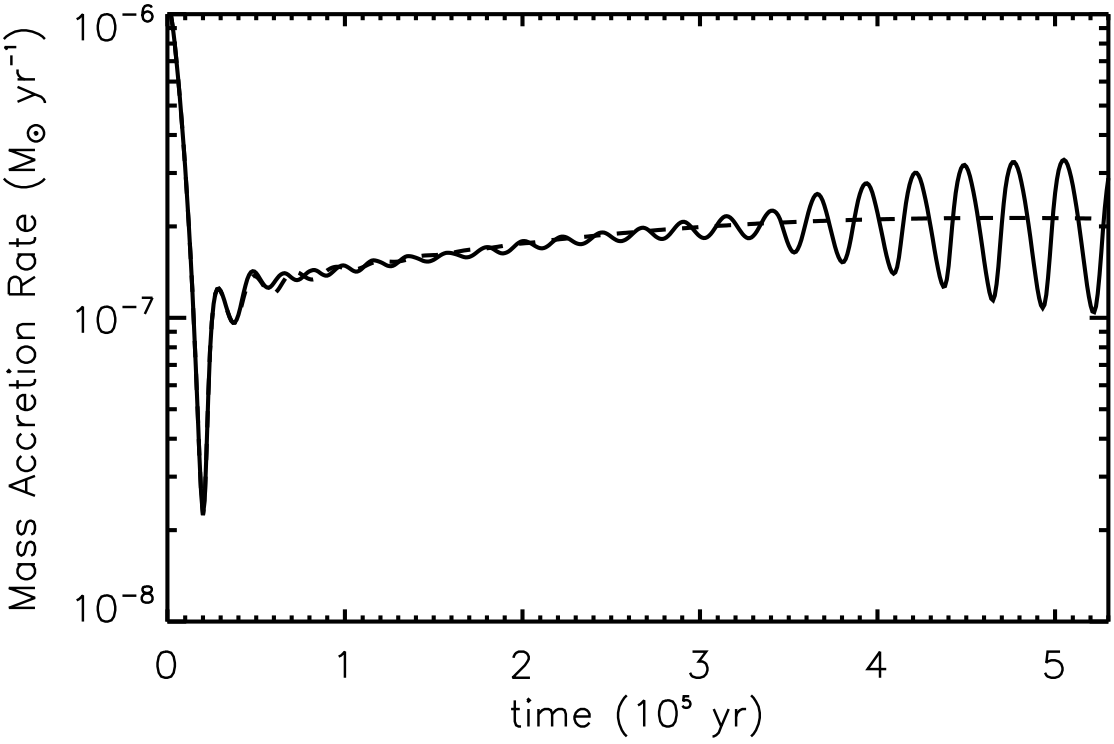


Fig. 5.— The mass accretion rate onto the star as a function of time. The solid curve indicates the mass accretion rate when feedback is included while the dashed curve neglects feedback.